Thermokinetic investigation of binary Cu/Zn hydroxycarbonates as precursors for Cu/ZnO catalysts

Andrey Tarasov, Julia Schumann, Frank Girgsdies, Nygil Thomas and Malte Behrens

Fritz Haber Institute of the Max-Planck Gesellschaft, Department of Inorganic Chemistry,

Faradayweg 4-6, 14195 Berlin (Germany)

Fax: (+49)30-8413-4401

tarasov@fhi-mpg.berlin.de

Keywords: Thermogravimetry, Cu/Zn hydroxycarbonates, decomposition kinetics

Abstract

A combination of thermogravimetric analysis (TG) and differential scanning calorimetry (DSC) coupled to mass spectrometry has been applied to study the thermal decomposition of Cu/Zn hydroxycarbonates, which are used as a precursor for the active methanol synthesis catalyst. Original TG and DSC profiles and results of a formal kinetic analysis of the calcination process are compared with transformations occurring in the solid phase, which has been studied by means of in-situ XRD. A series of hydroxycarbonate precursors with different Cu/Zn molar ratios (40/60, 60/40, 80/20) was synthesized under conditions reported as optimum for catalytic performance. The samples contain primarily two crystalline phases, aurichalcite $(Cu,Zn)_5(CO_3)_2(OH)_6$ and zincian malachite $(Cu,Zn)_2CO_3(OH)_2$. At least four formal decomposition stages of CO_2 and H_2O evolution cause the major mass loss in the TG experiments. The best-fit quality for the all studied samples was obtained for a four-step competitive reaction model. The experimental TG dependences are adequately described by the n-th order equation and 3D Jander diffusion equation. The effects of the gas flow, sample mass, and water transfer conditions on the reaction pathway were studied. The presence of H_2O vapor in the reaction feed accelerates the decomposition and dramatically changes the reaction TG profile. The decomposition enthalpy of mixed Cu/Zn (80/20) hydroxycarbonate was determined, and the formation enthalpy of the decomposition intermediate, a carbonate-modified oxide, was calculated to be ΔH_f^0=-633.7±5.6 kJ/mol.

1. Introduction

Recently, there has been a growing interest in the methanol synthesis and steam reforming of methanol reactions. Part of this interest stems from the projected methanol economy [1] and the increasing need for non-fossil fuels. Methanol can be used as a fuel in combustion engines and in methanol fuel cells or as a source of hydrogen for PEM fuel cells. It is also an important

feedstock for the synthesis of a variety of fine and bulk chemicals. Today, methanol is one of the top ten petrochemicals.

Ternary $Cu/ZnO/Al_2O_3$ systems are widely used in industry as catalysts for methanol synthesis and low-temperature water-gas shift reaction. The synthesis of such systems consists of a multi-step preparation route involving coprecipitation of mixed Cu/Zn hydroxyl-carbonate precursors, calcinations of these precursors to give a mixture of oxides and reduction of the CuO component. A vast number of studies on this system have shown that experimental conditions of each step significantly affect the microstructure, physicochemical properties and catalytic performance of $Cu/ZnO/Al_2O_3$ [2, 3, 4, 5]. However, different research groups have pointed out that the thermal activation has a pronounced effect on the porosity and structure of Cu-based catalysts. Reading and Dollimore [6] applied conventional rising-temperature thermogravimetry and introduced constant rate thermal analysis (CRTA) for examining the thermal decomposition of copper hydroxycarbonate. The development of the surface area as a function of the extent of decomposition was found to be markedly non-linear. The CRTA technique was used later for careful study of the decomposition mechanism of Cu/Zn hydroxycarbonates with different Cu-to-Zn ratio [7]. At the same time, the number of publications focusing on the description of the decomposition process and the influence of calcination conditions on the catalytic activity is quite limited [8, 9, 10, 11]. Some studies [12, 13] deal with the characterization of binary precursors for Cu/ZnO catalysts, which serve as a suitable model for technical ternary $Cu/ZnO/Al_2O_3$ systems.

Thermoanalytical studies often lack detailed information on reaction macrokinetics. To the best of our knowledge, the decomposition kinetics and dependence on reaction parameters, such as the mass of the precursor and gas-flow conditions, have not been reported for Cu/Zn hydroxycarbonates. The investigation of the decomposition kinetics provides better insight into transformations in the solid state upon heating and enables the optimization of the calcination protocol. These investigations help to design custom-made calcination protocols for individual samples, which in turn can be a determinative factor in catalytic activity.

The current work is aimed at studying the decomposition process of Cu/Zn hydroxycarbonates by means of coupled TG, DSC and MS techniques. The description of thermal events and the overall picture of calcination with respect to changes occurring in the solid and gas phases are also given. In addition, we performed the formal kinetic analysis of the calcination process of the mixed Cu/Zn hydroxycarbonates under recommendations of ICTAC (International Confederation for Thermal Analysis and Calorimetry) [14]. The TG and DSC profiles of the decomposition and the results of a kinetic analysis of the calcination process are compared with transformations taking place in the solid phase, by means of in-situ XRD.

2. Experimental

2.1 Sample Preparation

Cu/Zn precursors were prepared by pH-controlled coprecipitation [15] in an automated reactor (Mettler-Toledo LabMax). Different phases were prepared: aurichalcite (Cu:Zn, 40:60 molar ratio), zincian malachite (Cu:Zn, 80:20) and a phase mixture with a composition close to the industrially applied catalyst (Cu:Zn, 60:40). Appropriate amounts of $Zn(NO_3)_2$ $6H_2O$ and

$Cu(NO_3)_2 \cdot 3H_2O$ were dissolved in Millipore water (0.09µS/cm) and 15 ml of concentrated HNO_3 to obtain 600 ml of a 1 M solution of the metal salts. This solution was introduced into the reactor containing 400 ml of water at a constant rate of 20 ml/min. A 1.6 M Na_2CO_3 solution was automatically added to maintain constant pH 6.5. The precipitation temperature was 338 K. Precipitation was followed by ageing for 1 h (338K), after pH-drop. The solid was then filter-collected and washed several times by redispersion in water until the conductivity of the washing medium was below 0.5 mS/cm. The solid hydroxycarbonate precursors were obtained by spray drying.

2.2 XRD

XRD data were collected using a STOE STADI P transmission diffractometer equipped with a primary focusing Ge monochromator (Cu $K_{\alpha 1}$ radiation) and a linear position-sensitive detector (moving mode, step size 0.5 , counting time 30 s/step). The samples were mounted in the form of a clamped sandwich of small amounts of the powder fixed with a small amount of grease between two layers of a thin polyacetate film. The phase composition was determined by full pattern refinement in the 2θ range 4-80 according to the Rietveld method using the TOPAS software [16] and crystal structure data from the ICSD database.

Summarized crystallographic parameters of phases, the original XRD patterns and the results of Rietveld refinement are presented in supplementary information.

2.3 TG-MS

Simultaneous TG–DSC was carried out on a NETZSCH STA 449C Jupiter thermoanalyzer equipped with an electromagnetic microbalance with top loading. The TG resolution was 0.1µg. The relative error of mass determination was 0.5%. A highly sensitive sample carrier with Pt/Pt–Rh thermocouples was used. Measurements were taken in the temperature range 313–900K under a controlled Ar/O_2 flow 79:21 ml/min at a heating rate of 2, 5, 10 K/min. Gases used in the experiments were Ar (99.999%) and O_2 (99.999%). Samples of 10–15 mg were positioned into corundum crucibles (45 µl) without lids. Temperatures were calibrated against the melting points of In, Sn, Bi, Zn, Pb, Al and Au.

The gases evolved in the thermal analyses were monitored with a quadrupole mass spectrometer (QMS200 Omnistar, Balzers) coupled to STA via a quartz capillary heated to 313K. The experiments were performed with an electron ionization energy of 60 eV and a dwell time per mass of 0.2s. The main mass gates used were m/e 18 (H_2O), 28 (CO), 30 (NO), 32 (O_2), 44 (CO_2), and 46 (NO_2).

The experiments with sample loadings higher than 30 mg and with water vapor in the feed gas were performed on Rubotherm DynTherm Thermogravimetric Analyzer. The gas line was equipped with a saturator filled with water and held at room temperature.

For better quality of DSC curves, calorimetric experiments were carried out on a Mettler-Toledo HP DSC 827 calorimeter, with Au-AuPd Sensor, in 40-µl aluminum crucibles in a dynamic synthetic air (70 ml/min). Temperatures were calibrated against the melting points of In and Zn.

2.4 Kinetic Analysis

The kinetic data obtained in the experiments were processed using Netzsch software. The Proteus Thermal Analysis program was used for processing the raw TG and DSC curves, determining heats and mass changes, and smoothing and differentiating the curves. The integration of DSC heat effects was performed in the range of 400-720K, using tangential baseline. The Thermokinetics program was used for processing kinetic dependences and solving the direct and inverse kinetic problems. Eighteen different kinetic models were tested. For all models under consideration, a set of statistical criteria of adequacy was used according to the Netzsch procedure [17, 18]. The optimal model was selected on the basis of the discrepancies between the calculated and experimental values. The Peak Separation program was used for deconvolution of polymodal DSC peaks into components, processing TG curve derivatives, and searching for a best-fit function describing the peak shape. The reaction order parameter *n* was limited to a maximum value of 4±1.

2.5 In-situ X-ray diffraction

The *in-situ* XRD data were collected on a STOE Theta/theta X-ray diffractometer ($CuK\alpha_{1+2}$ radiation, secondary graphite monochromator, scintillation counter) equipped with an Anton Paar XRK 900 *in-situ* reactor chamber. The gas feed was mixed by means of Bronkhorst mass flow controllers, using helium as an inert balance gas at a total flow rate of 100 mln/min. The effluent gas composition was monitored with a Pfeiffer OmniStar quadrupole mass spectrometer. The dwell time on each temperature was 1.5 hr. The scan rate was 0.66 Θ/min.

3. Results and discussion

The crystalline components of the binary Cu/Zn hydroxycarbonates are related to the phases of zincian malachite [$M_2(CO_3)(OH)_2$] and aurichalcite $M_5(CO_3)_2(OH)_6$, where M is $Cu_xZn_{(1-x)}$ [12, 15]. The appearance of each phase depends on the Cu/Zn ratio, with a preference for zincian malachite at Zn contents lower than 30%, two-phase regime at 30 – 50% and aurichalcite above 50% [20]. In general, at least two main decomposition steps are involved in the TG decomposition pattern of these mixed hydroxycarbonates with Cu/Zn ratios ranging from 30/70 to 70/30 [11]. The first step (573-673K) is usually attributed to simultaneous evolution of CO_2 and H_2O, while the high temperature step (673-773K) is exclusively due to the release of CO_2. This “high-temperature carbonate” is thought of as a mixture of carbonates and oxides [19]. It is also known as anion-modified metal oxide $MO_{(1-y)}(CO_3)_{2y}$ and forms in the first step and decomposes to metal oxide afterwards [10, 20]. No such intermediate is observed for the non-mixed malachite and hydrozincite synthetic precursors [11], as well as for malachite minerals [12]. It is claimed in [21] that oxygen ions in this structure are substituted by OH^- and CO_3^{2-} groups, although the existence of OH-groups is questionable. To the best of our knowledge, its crystal structure has not been determined so far. Its abundance has been found to be a function of the Cu/Zn ratio and the hydroxycarbonate phase [11]. Calcination temperatures of catalytic precursors are usually within the range of 573-623 K [2, 3, 9]. Therefore, the carbonate-modified metal oxide can be trapped in the activated catalytic system, which in turn can influence the catalytic performance of these materials.

The most promising sample for thermokinetic study contains 40 mol% Cu and 60 mol% Zn (Cu/Zn/40/60). This is because of the fact that the above-mentioned thermal events in this sample are well resolved according to our experiments and the available literature data [11, 20]. The Rietveld refinement of XRD patterns indicates that the crystalline content of the material could be considered as a phase-pure aurichalcite. In addition, this precursor has the highest abundance of high-temperature carbonate compared to binary systems with other Cu/Zn ratios. Moreover, our tests showed that this sample exhibits high catalytic performance for methanol synthesis and the reverse water-gas shift reaction.

3.1 Thermogravimetric study and kinetic analysis.

The results of thermogravimetric analysis coupled with mass-spectrometry (TGMS) for the Cu/Zn/40/60 sample are shown in Figure 1. The shape of the DTG curve (Fig. 1) is in good agreement with the MS pattern indicating a decomposition process with at least four stages. The simultaneous and specific water and CO_2 evolution causes the main mass changes in the TG experiments.

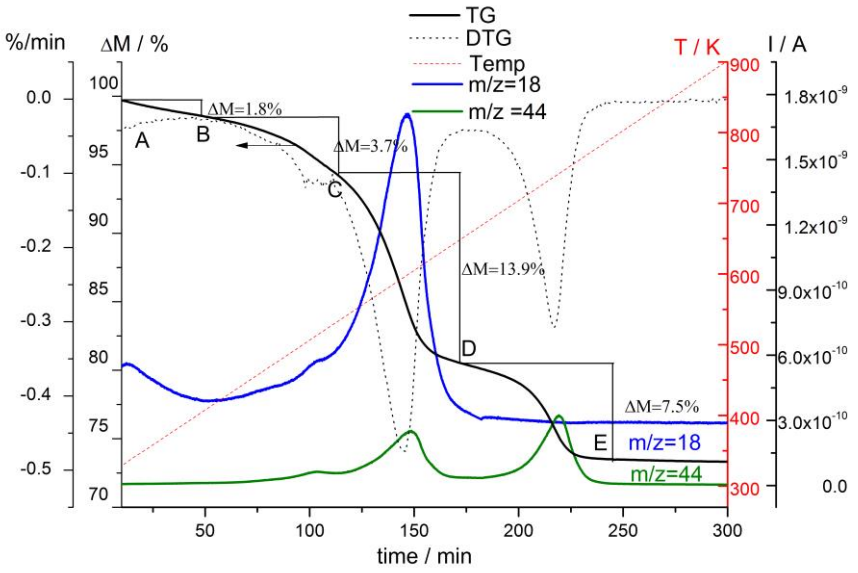

Fig1. TG and MS traces of H_2O, CO_2 recorded at 2K/min for precursor of Cu/Zn/40/60.

On heating the sample to 900 K, a steady mass loss is observed. This first segment on the TG curve (A to B) corresponds to a mass loss (ΔM) of 1.8%, which is due to desorption of adsorbed water from the surface of the precursor grains. The relatively high BET surface area of the sample (55 m^2/g) may explain the easy adsorption of physisorbed and free water molecules by the sample when contacted with ambient air. The mass loss of 3.7% at 400-550 (B to C) can be accounted for the loss of interlayer OH units. The 13.9% loss in the range 520-600K (C to D) is attributed to the decomposition of the main phase (aurichalcite) accompanied by strong simultaneous evolution of structural hydroxyl groups and carbonate units. The last decomposition step (D to E) shows a mass decrease of 7.5% in the range of 650-800K, which is accompanied by the release of only CO_2. The decomposition process of the pure aurichalcite phase to the oxides can thus be formally considered as a scheme of two consecutive reactions [20].

$$M_5(CO_3)_2(OH)_{6(s)} \rightarrow M_5O_4(CO_3)_{(s)} + 3H_2O_{(g)} + CO_{2(g)} \qquad \Delta m_{theory}=18.0\% \ (1)$$

$$M_5O_4(CO_3)_{(s)} \rightarrow 5MO_{(s)} + CO_{2(g)}, \quad \text{where } M=Cu_{0,4}Zn_{0,6} \qquad \Delta m_{theory}=8.2\% \ (2)$$

Figure 2 shows a set of TG curves recorded at different heating rates. An extra measurement at a heating rate of 20 K/min was carried out in order to elucidate the effect of heating rate. This experiment was not considered in further non-isothermal kinetic analysis. With an increase in the heating rate, reaction (1) (including stages A to D) is shifted to higher temperatures more than reaction (2) (stages D to E), causing slight overlapping of the two mass loss steps. Since both steps shift during the process, reactions (1) and (2) can be considered to be consecutive. It is expected that at higher heating rates there is an increasing overlap of the two steps. The reaction rate of the second step cannot exceed the reaction rate of the first step; hence, the first step is the limiting step for the second step. Formally, for very high heating rates, the rates of reactions (1) and (2) will be equal, the concentration of intermediate high-temperature carbonate will be about zero, and the two-step process will look like a single-step process, which produces a one-step TG curve containing no information about the kinetics of the second step [22].

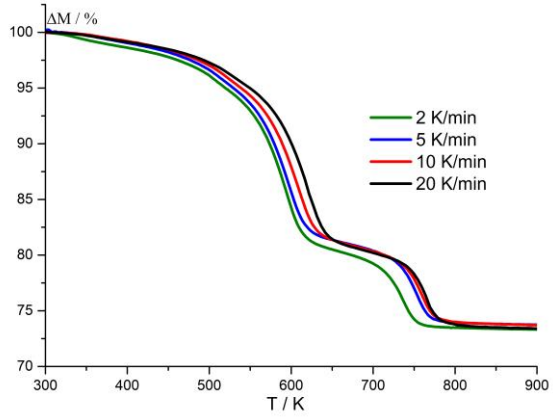

Fig. 2. Thermogravimetric curves at 2, 5, 10 and 20 K/min, 21% O_2 in Ar.

3.2 Influence of mass-transfer

Decomposition profiles are strongly dependent on the sample mass. Figure 3 shows the influence of the sample loading on the decomposition pattern. The decomposition behavior of the last step completely changes with variation of sample mass. (Fig. 3). As the sample amount increases from 10 to 300 mg, the mass loss of the decomposition of the intermediate high-temperature carbonate decreases (a lower CO_2 evolution during step 2 according to the mass spectrum). The decomposition patterns have an identical behavior until a degree of reaction of ca. ΔM=15%. All major differences are observed in the temperature range of high-temperature carbonate decomposition, indicating that mass transfer conditions affect this process. It was noted by Fujita et al. [10] that the presence of water in the gas stream during calcination increases the rate of copper oxide crystallite growth. Most probably, higher loadings cause a transfer

limitation of water removal, which increases the local water concentration above the sample and changes the reaction pathway. The effect was studied in detail for the decomposition process of $Mg(OH)_2$ [23]. The continued presence of water molecules on, or in close proximity to, the MgO surface at temperatures above that decomposition leads to enhanced crystal growth and agglomeration by increased surface diffusion. In order to verify the role of water on the high-temperature carbonate formation, we performed an additional experiment with water in the feed gas.

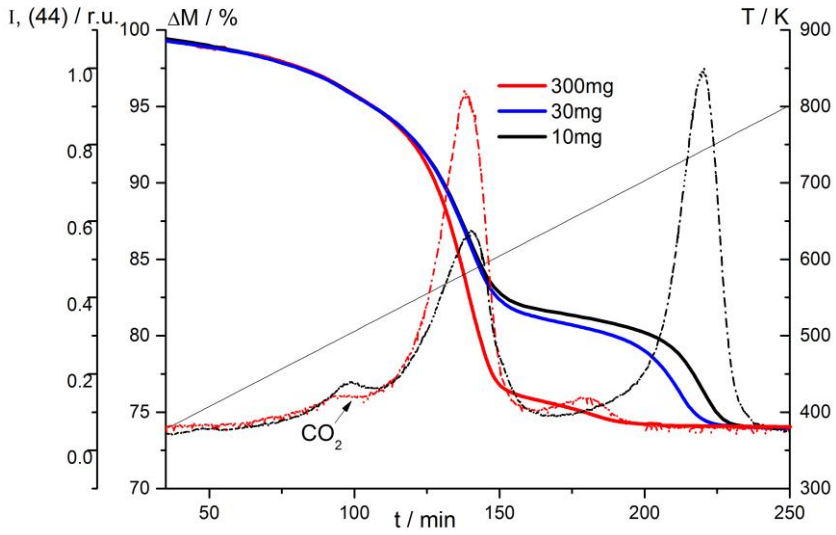

Fig. 3. TG curves and MS traces of CO_2 recorded at 2 K/min for precursor of Cu/Zn/40/60, 100 ml/min, 21% O_2 in Ar

The decomposition behavior of *Cu/Zn/40/60* with addition of water vapor to the feed gas is shown in Figure 4. The presence of water in the gas atmosphere clearly accelerates the decomposition process and completely suppresses the formation of the intermediate high-temperature carbonate.

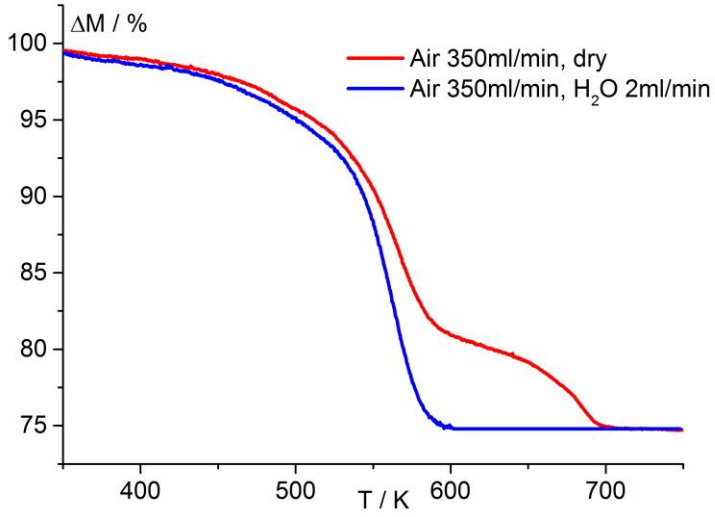

Fig. 4. TG profiles of the Cu/Zn/40/60 precursor without water (red) and with 0.5% water vapor in the gas feed (blue).

Based on the above findings, a formal reaction scheme is proposed (Fig. 5). The reaction follows the direct formation of oxide (k1) when there is water transfer limitation and runs through the formation of an intermediate carbonate-modified oxide (k2) only when water is removed readily from the sample according to consecutive reactions (1) and (2). The conditions can be tuned so that these formal reactions would take place with equal probability. Thus, a competitive reaction model can be applied. It should be noted that the reaction model does not imply the back reaction. It is quite possible that there is a reformation of carbonate in steam or a formation of hydroxide under the conditions of local water pressure. These processes cannot be ruled out since there was no experimental possibility for proving their absence under non-dry conditions.

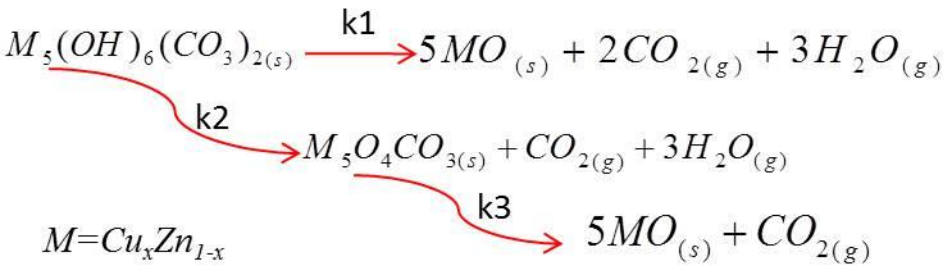

Fig. 5. Suggested reaction scheme of aurichalcite decomposition.

3.3 Thermokinetic analysis

The decomposition behavior of the precursor indicates the presence of overlapping regions between successive stages. The solution of the inverse kinetic problem by the Flynn-Wall-Ozawa (FWO) method, with use of the Thermokinetic program package, confirmed the existence of at least four stages for the entire process (Fig. 6); however, the first two steps are strongly overlapped. The obtained values were used later as initial kinetic parameters for the NLR method.

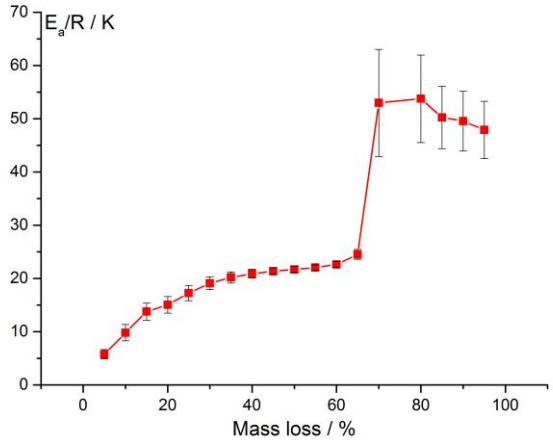

Fig. 6. FWO calculation: activation energy as a function of conversion

Critical abundance of an intermediate on each stage is necessary to initiate the nucleation of the product. Thus, the kinetics cannot be considered as separate subsequent stages. In case of a process with consecutive and parallel stages, as can easily occur in decomposition reactions, possible errors in estimation of kinetic parameters will be substantial. Since the crystal structures of all compounds of relevance are different, the topotactic reactions are difficult to assume, and the whole curve may be represented as a superposition of single-step decomposition processes. The entire process, including the desorption of adsorbed water, is mathematically represented by five successive stages A-E (Fig. 1) separated by the four DTG peaks 1-4 as shown in Figure 7. Each peak is considered as a quasi-single-step process. Integration of each peak enables to obtain a set of kinetic curves for each stage.

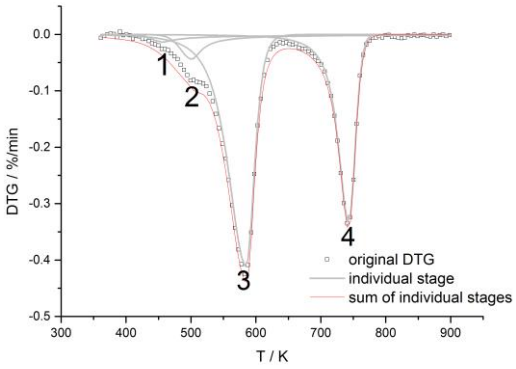

Fig. 7. Derivative of TG curve mathematically separated into components.

Partial areas of separated peaks were constant within the error margin for every heating rate, which implies that the pathway of the process remains unchanged and confirms the decomposition as a superposition of four limiting stages (Table 1).

Table 1. Partial peak areas of DTG curves under different heating rates

Number of DTG peak	2K/min	5K/min	10K/min
1	0.02	0.02	0.02
2	0.22	0.24	0.23
3	0.47	0.46	0.50
4	0.29	0.28	0.25

The kinetic parameters of each step were determined using the model-free isoconversional (FWO) method and were refined using a non-linear regression (NLR) least-squares procedure for different types of conversion functions f(α).

The change in the decomposition rate as a function of temperature can be described with Arrhenius non-isothermal equation (3) as follows

$$-\frac{d\alpha}{dT} = \frac{A}{\beta} e^{-Ea/RT} f(\alpha) \qquad (3),$$

where *A* is the preexponential factor in s^{-1}, E_a is the activation energy in kJ/mol, T is the temperature in kelvins, β=*dT/dt* is the heating rate in K/min, and f(α) is some function of the conversion of the reaction characterizing its mechanism. The conversion **α**, is defined as the fraction of the initial reagent A that has decomposed by time t and changes from 0 to 1.

The experimental DTG curves for the first, second and third stages are reliably described by the n-th order reaction equation $f(\alpha) = (1-\alpha)^n$, while the best-fit curve for the fourth step is obtained using the 3-dimensional Jander-type diffusion equation $f(\alpha) = 3(1-\alpha)^{2/3}/2(1-(1-\alpha)^{1/3})$. Kinetic parameters calculated for each step were used as starting parameters for non-linear regression optimization of the whole DTG curve. Several combinations of parallel, competitive and consecutive processes were used, and fit qualities were determined for each model. The fitting procedure has been well described in [17]. Statistical comparison of the fit quality for different models was estimated by means of Fisher test. The best fit corresponds to the four consecutive reaction model, shown in Figure 8.

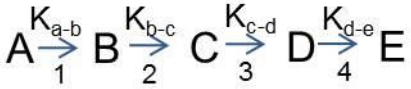

Fig. 8. Consecutive reaction model.

According to this formal scheme, the reaction runs through the formation of kinetically stable intermediate (carbonate-modified oxide or high-temperature carbonate). Kinetic parameters for each stage of the whole curve are listed in Table 2. The values in the table are in good agreement with the results of OFW calculation. It is worth noting that kinetic parameters for individual steps of the whole curve differ from those obtained for separate curves (Table 1).

However, the type of conversion functions remains the same, which supports the suggested decomposition model.

Table 2. Kinetic Parameters for decomposition of aurichalcite precursor obtained using 4-step consecutive reaction model

Stage No	E_a/R *10^3 K	*Pre-exponential factor,* $\log A_i$	*Reaction order,* n_i
1	4.8±1.2	2.6±0.2	1.4±0.5
2	19.1±5.5	14.1±3.1	4.4±1.3
3	21.8±5.0	13.8±3.6	1.8±0.4
4	55.8±8.6	29.0±5.1	

The experimental TG curves at different heating rates (2, 5, 10 K/min) and the fitted patterns are shown in Figure 9. The deviation of the mass loss obtained at different heating rates is very low, approximately 1%. The mass change of the last carbonate decomposition step is independent of the heating rate. It follows from Table 2 that the dehydration kinetics and desorption of weakly bonded water species are close to the 1st order equation.

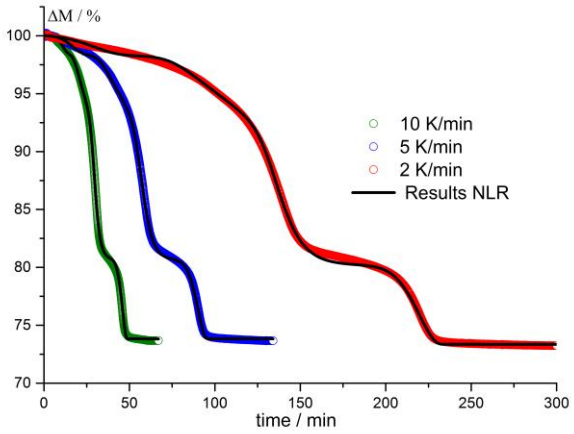

Fig. 9. Experimental TG curves and results of NLR for the aurichalcite precursor.

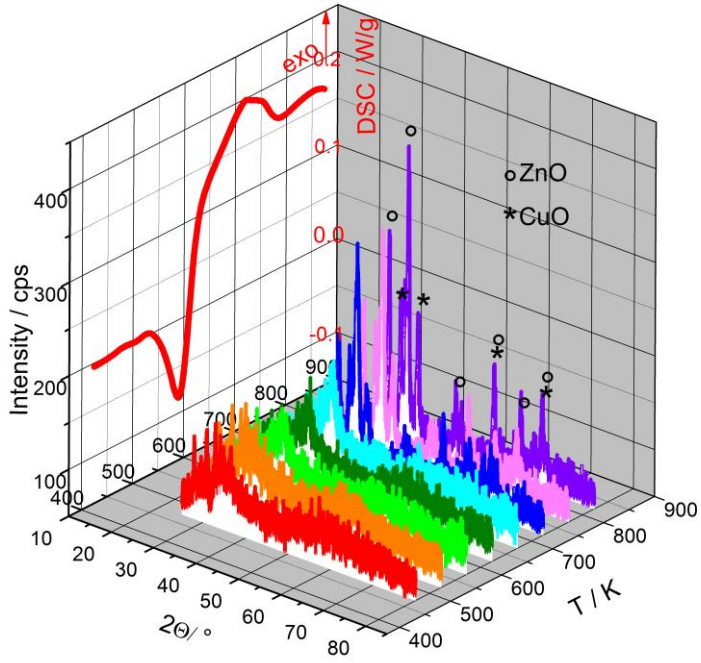

Fig. 10. Three-dimensional representation of combined XRD-DSC plots for the precursor Cu/Zn=40/60, calcination in 21% O_2 in Ar.

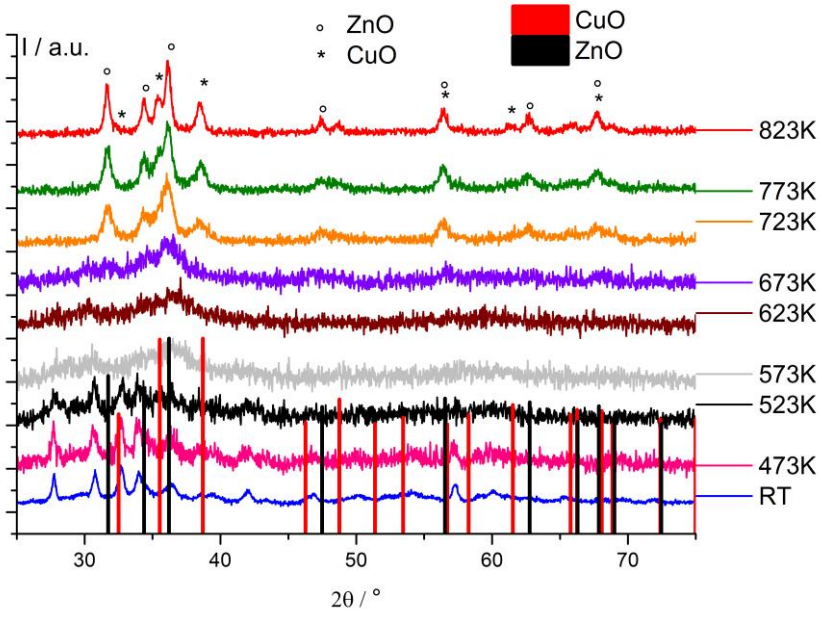

Fig. 11. In-situ XRD patterns upon decomposition of the precursor Cu/Zn=40/60, 21% O_2 in Ar.

In two aurichalcite decomposition stages 2 and 3, the temperature rate coefficients (Ea/R), as well as pre-exponential factors (Table 1), are similar. However, the reaction order decreases from stage 2 to 3, which is probably due to the decrease in the nucleation rate [24]. The obtained kinetic parameters agree with the values for the pure malachite [25] and zinc carbonate hydroxide, hydrozincite [26]. It should be noted that the performed analysis reveals the formal

macrokinetic mechanism. The formal model that describes the process kinetics and the real reaction mechanism are certainly close to each other but are not the same. For polydisperse systems in which parallel processes occur, microkinetic modeling is a rather challenging task, so that it is better to use a physical and mathematical description of the overall process. The formal reaction steps represent composite reactions themselves. There could be elementary steps (not considered) which lead to certain numerical deviations of the determined formal kinetic parameters. However, the DTG peaks do not necessarily correspond to single stoichiometric steps. There might be a number of steps regulated by changing geometry of the solid interface upon heterogeneous decomposition within one stoichiometric reaction.

We performed an in-situ XRD experiment in order to follow the structural changes of the material under heating. Figure 10 shows the three-dimensional representation of combined XRD-DSC data of Cu/Zn/40/60 at different temperatures. The XRD patterns are also shown in Figure 11. The changes of diffraction intensities in the XRD patterns are quite consistent with the DSC curve. Note that, in the XRD experiment, the dwell time at each temperature was two hours, while the DCS curve was recorded at a constant heating rate. It seems doubtful to interpret the mechanistic aspects relying on XRD data; however, it can provide supportive information about stable solid products appearing upon the decomposition proccess. The particular area of interest was between 573 and 673K (Fig. 1) where the high-temperature carbonate was observed. It can be seen (Figs. 10, 11) that, in this temperature range, a phase of missing long-range order is formed. The formation of intermediate high-temperature carbonate is accompanied by an endothermic event, with a peak maximum around 623K, corresponding to DTG peak #3. It can be clearly observed that the change in XRD patterns gradually starts from 673K towards the formation of crystalline oxides, ZnO and CuO, and is accompanied by an exothermic effect corresponding to DTG peak #4 as expected for the crystallization event. Based on the kinetic data from Table 3, this step is characterized by a high value of Ea/R and fits well with Jander's diffusion equation [27]. Upon decomposition of the carbonate-modified oxide phase, ZnO starts to crystallize. The rest of carbonate decomposes and evolves CO_2, initiating crystallization of copper oxide. At ~723K, the reflections of copper oxide appear. A very high activation barrier features this stage (Table 2). According to Jander's original work [27], this stage of decomposition describes reactions limited by diffusion in the solid state. A likely interpretation is that, upon decomposition of high-temperature carbonate, the zinc atoms leave the shared positions in the lattice and diffuse through the solid to form zinc oxide. Simultaneously, the rest of carbonate decomposes during the crystallization of copper oxide and zinc oxide. Further heat treatment of the CuO and ZnO formed results in crystal growth through material transport and sintering together of the oxide crystals [28].

The mathematical models used for the description of the mechanism are based on the assumption of ideal spherically shaped particles. The reaction rate is either regulated by the surface of unreacted particles, as for the n-th order equation, or limited by diffusion through the formed solid product, as for the Jander diffusion. These equations were successfully applied for description of mechanistic aspects of decomposition kinetics for a variety of inorganic substances

[29]. However, the quality of fitting and the appropriateness of the mechanism strongly rely on the physicochemical basis of kinetic modeling.

3.4 Decomposition of a zincian malachite precursor with the 80-to-20 copper-to-zinc ratio

The same approach and procedure was applied to study the decomposition of the Cu/Zn/80/20 sample with a Cu:Zn ratio of 80:20. This composition is much closer to the Cu:Zn ratio applied for catalyst synthesis. According to the Rietveld refinement of the XRD pattern of this sample, the precursor consists of 100% zincian malachite. This sample is characterized by well-defined decomposition steps (Fig. 12). However, the high-temperature carbonate decomposition step is not so well resolved and strongly overlaps with the previous decomposition step.

As in the case of Cu/Zn/40/60, the experimental curves for the first, second and third stages were reliably described by the n-th order reaction equation. The best-fit curve for the fourth stage was again obtained using the three-dimensional Jander-type diffusion equation (Fig. 12). However, for this Cu-rich sample, the most reliable fit is obtained using the 2 consecutive and 3 competitive reactions model, where every letter of the formal reaction model (Fig. 13) meets the corresponding solid substance on the suggested branching reaction scheme (Fig. 14). In contrast to calcined aurichalcite samples, XRD showed the presence of the CuO phase in the malachite precursors calcined at 603K and 2 K/min, indicating earlier crystallization of oxides before decomposition of intermediate carbonate. One should point out that the prerequisite for parallel reactions is the dependence of the total mass loss of the reaction on heating rates. However, the competitive steps of formation of high temperature carbonate C → D and direct formation of oxides C → F are a part of the consecutive reaction model (Fig. 13) where final products E and F have identical chemical composition. For consecutive steps, the total effect of reaction is always the same [22] for any heating rate; thus, the shift of the mass loss of the intermediate stage is slightly pronounced.

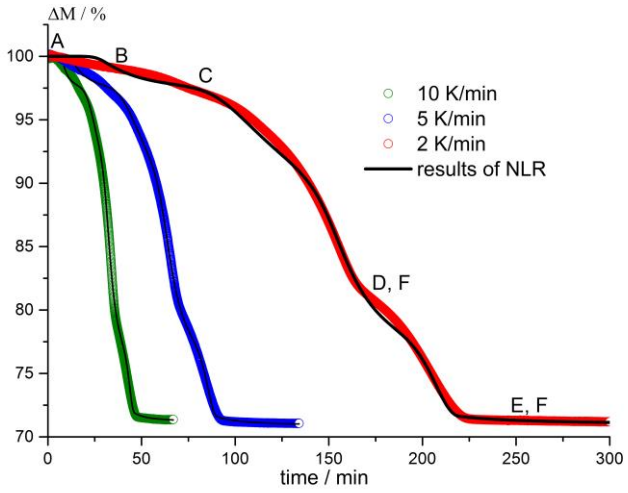

Fig. 12. TG curves and results of NLR of zincian malachite precursor decomposition (Cu/Zn/80/20).

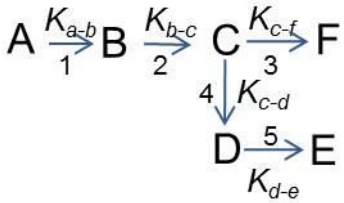

Fig. 13. Formal kinetic model with 2 Consecutive and 3 competitive reactions

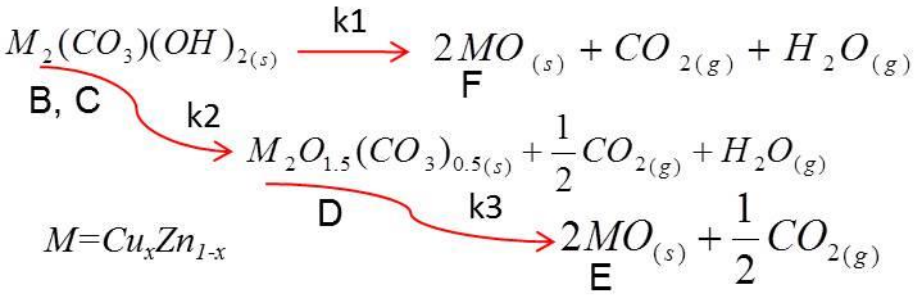

Fig. 14. Suggested reaction scheme of zincian malachite decomposition

Table 3. Kinetic Parameters for decomposition of the Cu/Zn/80/20 precursor

Stage No	E_a/R *10^3 K	*Pre-exponential factor,* $\log A_i$	*Reaction order,* n_i
1	6.9±1.4	5.0±0.4	1.6±0.2
2	21.1±6.2	15.9±0.2	3.7±0.7
3	29.6±6.4	18.9±0.5	3.3±0.2
4	11.2±0.5	6.1±0.2	5.7±1.0
5	35.7±7.0	18.1±0.3	

It should be noted that F and E appear to be the same chemical product, a mixture of the simple oxides, but formed via different routes. The kinetic parameters of zincian malachite decomposition are summarized in Table 3. The first stage of water desorption has approximately the same kinetic parameters as previously observed for the aurichalcite phase. The competitive reaction k3 is characterized by the drop of temperature rate coefficient Ea/R. However, the second simultaneous decomposition step (stage number 2) has a high activation barrier and tends to be the rate-limiting stage of the process. The activation energy of decomposition of high-temperature carbonate, 297 kJ/mol, is lower than for aurichalcite, 406 kJ/mol; therefore, the intermediate high-temperature carbonate state is less stable in zincian malachite. This is likely related to its decomposition with evolution of a higher water amount per mole of metal oxide (MO/H_2O=2, Fig. 14) as compared with aurichalcite (MO/H_2O=1.7, Fig. 5). This results in a lower thermal stability of the intermediate and a higher contribution of reaction 3 with direct formation of metal oxide. It is worth noting that the explanation is rather rough since the atomic properties are interpretable when they completely refer to elementary reactions. It should be noted that direct comparison of activation energies for two processes could be implemented if only other parameters of the kinetic triplet, namely, the pre-exponential factor *A* and the type of conversion function *f(α)*, are the same.

3.5 Comparative thermochemical study of mixed Cu,Zn hydroxycarbonates.

The DSC experiment was performed simultaneously with TG measurements on the precursors with different Cu-to-Zn ratios, Cu/Zn/40/60, Cu/Zn/80/20 and Cu/Zn/60/40, representing aurichalcite (see sections 3.1-3.3), zincian malachite (see section 3.4), and a phase mixture thereof (Fig. 15). In all cases, the main mass loss in the range 600-700K is accompanied by an endothermal transformation (formation of high-temperature carbonate) followed by a broad exotherm of crystallization of oxide products (decomposition of high-temperature carbonate). The exothermal event is linked to the final decarbonation mass loss in the range 700 –800K. As can be seen from figure 15, upon decreasing the Zn content, the position of the endothermic peak shifts 30K towards higher values, which is thought to be related to the crystallinity of the hydroxycarbonates [7]. Table 4 summarizes the enthalpies of decomposition of Cu/Zn precursors. The experimental mass loss for the second step is given for the conditions with a heating rate of 10 K/min. With an increase in the amount of Zn-O bonds, the endothermic effect grows. This is in good agreement with the expected trend since the enthalpy of Zn-O bond cleavage (282.0 kJ/mol) is slightly higher than the Cu-O bond energy (266.7 kJ/mol) [30].

Table 4. Decomposition enthalpies of different Cu/Zn precursors. Integration of DSC curves (Fig. 15) performed in the temperature range 425-725K

Cu/Zn (mol)	ZM, wt %	AC, wt %	ΔH°_{d}, kJ/mol*	CO_2 from HT-CO_3, wt %		Nominal precursor composition
				experiment	theory	
80/20	100	0	75.0±4.0	8.3	10.0	$(Cu_{0.8}Zn_{0.2})_2(CO_3)(OH)_2$
60/40	80	20	113.3±6.0	8.2	9.4	$0.8(Cu_{0.6}Zn_{0.4})_2(CO_3)(OH)_2$+$0.2(Cu_{0.6}Zn_{0.4})_5(CO_3)_2(OH)_6$
40/60	0	100	280.0±15.0	7.1	8.2	$(Cu_{0.4}Zn_{0.6})_5(CO_3)_2(OH)_6$

*mole of corresponding hydroxycarbonate.

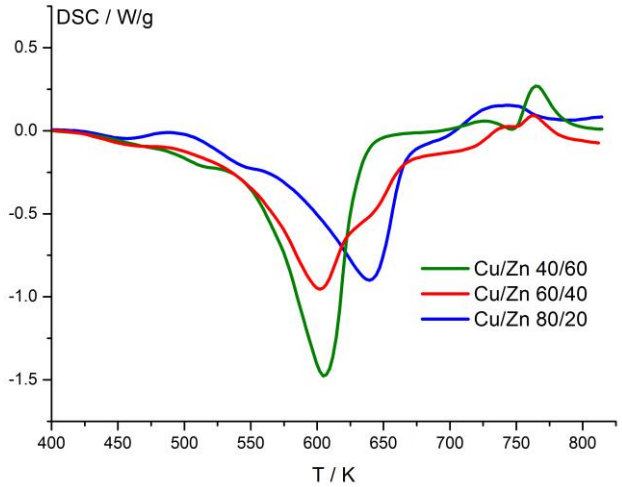

Fig. 15. DSC curves of precursors containing 20, 40 and 60 mol % Zn, recorded at a heating rate of 10 K/min

The effect of different amounts of carbonate-modified oxide (or high-temperature carbonate) on the decomposition enthalpy was studied on the phase-pure zincian malachite sample $(Cu_{0.8}Zn_{0.2})_2(CO_3)(OH)_2$. The amount of high-temperature carbonate formed was controlled by

varying the sample mass from 10 to 30 mg. An increase in the sample mass causes additional water transfer limitation, which accelerates the decomposition resulting in a lower content of carbonate-modified oxide, as described in section 3.2 for aurichalcite. The decomposition enthalpy depends linearly (Fig. 16) on the resulting carbonate-modified oxide content. Thus, for the 0 wt% of high-temperature carbonate, the enthalpy of decomposition of the zincian malachite precursor is 89.0 ± 4.7kJ/mol, which is in agreement with the theoretical value of 85.0±3.1kJ/mol and with the values for Cu malachite and azurite [31]. The theoretical value of the enthalpy of formation of $(Cu_{0.8}Zn_{0.2})_2(CO_3)(OH)_2$ was calculated as the sum of the decomposition enthalpies of pure substances (carbonates and hydroxides) in the following proportion: $0.8\Delta H_f(CuCO_3)+0.8\Delta H_f(Cu(OH)_2)+0.2\Delta H_f(ZnCO_3)+0.2\Delta H_f(Zn(OH)_2)$. The enthalpy of decomposition was calculated as follows: $1.6\Delta H_f(CuO)+0.4\Delta H_f(ZnO)+\Delta H_f(H_2O)+\Delta H_f(CO_2)-\Delta H_f(Cu_{0.8}Zn_{0.2})_2(CO_3)(OH)_2$

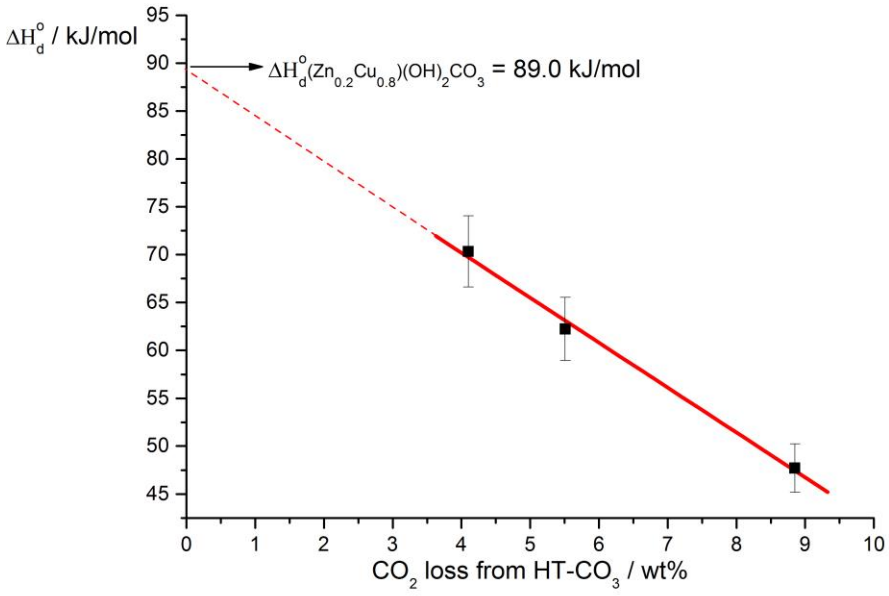

Fig. 16. Dependence of the decomposition enthalpy of zincian malachite (Cu/ZnO/80/20) on the high-temperature carbonate content formed during decomposition in the first step.

The maximum amount of HT-CO_3 according to the reaction scheme (Fig. 14) would result in the mass loss of CO_2 of 10% upon decomposition (Table 5). Assuming linearity of the function (Fig. 16), the decomposition enthalpy would be 42 kJ/mol. Simple calculation using the experimentally determined enthalpies of decomposition of the zincian malachite precursor that occurs with and without formation of HT-CO_3 (89kJ/mol and 42kJ/mol) and the known standard enthalpies of the reactants for CuO $\Delta H_f^0{}_{,298.15}$=-156.1±2.1, ZnO $\Delta H_f^0{}_{,298.15}$=-350.5±0.3kJ/mol and CO_2 $\Delta H_f^0{}_{,298.15}$=-393.5±2.1 allows to assess the enthalpy of formation of carbonate-modified oxide $(Cu_{0.8}Zn_{0.2})_2O_{1.5}(CO_3)_{0.5}$: ΔH_f^0=-633.7±5.6kJ/mol. The calculation was performed assuming that the formation enthalpy is temperature independent.

4. Conclusions

The high-temperature carbonate, or carbonate-modified oxide, is a kinetically stable intermediate, which specifically forms upon decomposition of mixed (Cu, Zn) hydroxycarbonates. The appearance of the additional decomposition step is explained by limitation caused by crystallization and segregation of zinc and copper oxides. The stability of this high-temperature carbonate directly depends on water transfer conditions, and the decomposition of this phase was found to be accelerated by adding water vapor in the feed or by increasing the precursor loading. Kinetic parameters of the decomposition process of two structurally different Cu/Zn hydroxy-carbonates (aurichalcite and zincian malachite) were determined and verified. On the basis of the kinetic evaluations of the decomposition behavior and from in-situ XRD measurements, a possible reaction scheme was suggested. In the process of Cu/ZnO catalyst synthesis, the obtained kinetic values allow controlling the degree of decomposition and the reaction rate during calcination. A study of the relevance of these effects and of the amount of high-temperature carbonate in calcined catalysts will be presented elsewhere.

Acknowledgments

We thank Prof. Robert Schlögl for fruitful discussions and continuous support. We express sincere gratitude to Dr. Gayana Kirakosyan for useful remarks and stylistic advice.

References

[1] G. A. Olah, A. Goeppert, GKS. Prakash, Beyond oil and gas: the methanol economy. Weinheim an der Bergstrasse, Germany: Wiley.VCH; 2006.

[2] C. Baltes, S. Vukojevic, F. Schüth, Correlations between synthesis, precursor, and catalyst structure and activity of a large set of $CuO/ZnO/Al_2O_3$ catalysts for methanol synthesis, Journal of Catalysis 258 (2008) 334-344.

[3] M. Behrens, I. Kasatkin, S. Kühl, G. Weinberg, Phase-Pure Cu,Zn,Al Hydrotalcite-like Materials as Precursors for Copper rich $Cu/ZnO/Al_2O_3$ Chem. Mater. 22 (2010) 386-397.

[4] S. Kaluza, M. Behrens, N. Schiefenhövel, B. Kniep, R. Fischer, R. Schlögl, M. Muhler, A Novel Synthesis Route for $Cu/ZnO/Al_2O_3$ Catalyst in Methanol Synthesis: Combining Continuous Consecutive Precipitation with Continuous Aging of the Precipitate, ChemCatChem 3 (2011) 189-199.

[5] M. Schur, B. Bems, A. Dassenoy, I. Kasatkine, J. Urban, H. Wilmes, O. Hinrichsen, M. Muhler, R. Schlögl, Continuous Coprecipitation of Catalysts in a Micromixer: Nanostructured Cu/ZnO Composite for the Synthesis of Methanol Angew. Chem. Int. Ed. 42 (2003) 3815-3817.

[6] M. Reading, D. Dollimore, The application of constant rate thermal analysis to the study of the thermal decomposition of copper hydroxy carbonate, Thermochemica Acta, 240 (1994) 117-127.

[7] V. Vagvölgyi. A Locke, M. Hales, J. Kristof, R. L. Frost, E. Horvath, W. N. Martens, Mechanism for decomposition of aurichalcite – A controlled rate thermal analysis study, Thermochemica Acta 468 (2008) 81-86.

[8] M. J. L. Gines, C. R. Apesteguia, Thermal decomposition of Cu-based Hydroxycarbonate Catalytic Precursors for the Low-Temperature Co-Shift Reaction, J Therm Anal Calorim 50 (1997) 745-756.

[9] S. Fujita, S. Moribe, Y. Kanamori, M. Kakudate, N. Takezawa, Preparation of a coprecipitated Cu/ZnO catalyst for the methanol synthesis from CO2—effects of the calcination and reduction conditions on the catalytic performance, Applied Catalysis A: General 207 (2001) 121-128.

[10] S. Fujita, S. Moribe, Y. Kanamori, M. Kakudate, N. Takezawa, Effects of The Calcination and Reduction Conditions on a Cu/ZnO Methanol Synthesis Catalyst, React. Kinet. Catal. Lett. 70 (2000) 11-16.

[11] B. Bems, M. Schur, A. Dassenoy, H. Junkes, D. Herein, R. Schlögl, Relations between Synthesis and Microstructural Properties of Copper/Zinc Hydroxycarbonates Chem. Eur. J. 9 (2003) 2039-2052

[12] M. Behrens, F. Girgsdies, A. Trunschke, R. Schlögl, Minerals as Model Compounds for Cu/ZnO Catalyst Precursors: Structural and Thermal Properties and IR Spectra of Mineral and

Synthetic (Zincian) Malachite, Rosasite and Aurichalcite and a Catalyst Precursor Mixture, Eur. J. Inorg. Chem. (2009) 1347-1357

[13] B. J. Reddy, R. L. Frost, A. Locke, Synthesis and spectroscopic characterization of aurichalcite $(Zn,Cu^{2+})_5(CO_3)_2(OH)_6$; implications for Cu-ZnO catalyst precursors, Transition Met Chem 33 (2008) 331-339.

[14] S. Vyazovkin, A. K. Burnham, J. M. Criado, L. A. Pérez-Maqueda, C. Popescu, N. Sbirrazzuoli, ICTAC Kinetics Committee recommendations for performing kinetic computations on thermal analysis data, Thermochim. Acta *520 (*2011) 1–19.

[15] M. Behrens, Meso- and nano-structuring of industrial Cu/ZnO/(Al2O3) catalysts, J. Catal. 267 (2009) 24-29.

[16] A. Coelho TOPAS Karlsruhe, Germany, Bruker AXS GmbH, 2003-2009.

[17] J. Opfermann, Kinetic Analysis Using Multivariate Non-linear Regreassion, J Therm Anal Calorim 60 (2000):641–658.

[18] I. V. Arkhangelsky, A. V. Dunaev, I.V. Makarenko, N. A. Tikhonov, S. S. Belyaev, and A. V. Tarasov. Non-Isothermal Kinetic Methods. Workbook and Laboratory Manual. Berlin, Germany: Edition Open Acces; 2013.

[19] R. L. Frost, A. J. Locke, M. C. Hales, W. N. Martens, Thermal stability of synthetic aurichalcite implications for making mixed metal oxides for use as catalyst, J. Therm. Anal. Calorim. 94 (2008) 203-208.

[20] G.J. Millar, I. H. Holm, P.J . Uwins, J. Drennan, Characterization of precursors to methanol synthesis catalysts Cu/ZnO system J. Chem. Soc. Faraday Trans. 94 (1998) 593.

[21] T.M. Yurieva, Catalyst for methanol synthesis: preparation and activation, React. Kinet. Catal. Lett. 55 (1995) 513-521.

[22] E. Moukhina, Determination of kinetic mechanisms for reactions measured with thermoanalytical instruments, J Therm Anal Cal 109 (2012) 1203-1214.

[23] J. Green, Calcination of precipitated $Mg(OH)_2$ to active MgO in the production of refractory and chemical grade MgO, J Mater Sci 18 (1983) 637-651.

[24] B. Delmon. Introduction to Heterogeneous Kinetics. Paris: Technip, 1969.

[25] S.A.A. Mansour, Thermoanalitical Investigations of Decomposition Course of Copper Oxysalts, J Therm Anal Calorim 42 (1994) 1251-1263.

[26] A.H. Nobari, M. Halali, An investigation on the calcination kinetics of zinc carbonate hydroxide and Calsimin zinc carbonate concentrate, Chemical Engineering Journal, 121 (2006) 79-84.

[27] W. Jander, Reaktionen im festen Zustände bei höheren Temperaturen, Würzburg, Chemische Institut der Universität, 1927.

[28] L. Markov, R. Ioncheva, Synthesis and Thermal Decomposition Of Cu(II)-Zn(II) Hydroxide Nitrate Mixed Crystals, Mater. Chem. Phys. 26 (1990) 493-504.

[29] Sestak J. Thermophysical properties of solids. Academia Prague. 1984.

[30] Energii razryva khimicheskikh svyazei, potentsialy ionizatsii i srodstvo k elektronu: Sparvochnik (Bond Energies, Ionization Potentials, and Electron Affinities: A Handbook, Kondrat'ev, V.N., Ed., Moscow: Nauka, 1974.

[31] I. A. Kiseleva, L. P. Ogorodova, L. V. Melchakova, M. R Bisenglieva and N. S. Becturganov, Thermodynamic Properties of Copper Carbonates-Malachite $Cu_2(OH)_2CO_3$ and Azurite $Cu_3(OH)_2(CO_3)_2$, Phys Chem Minerals 19 (1992) 322-333.

Supplementary information.

Rietveld refinements.

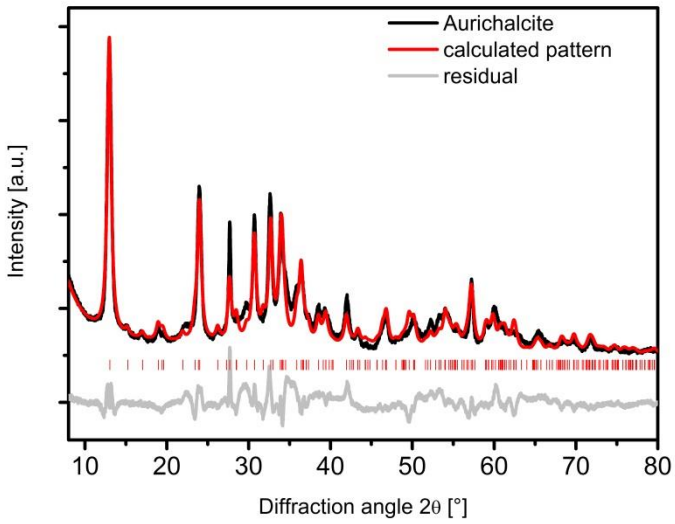

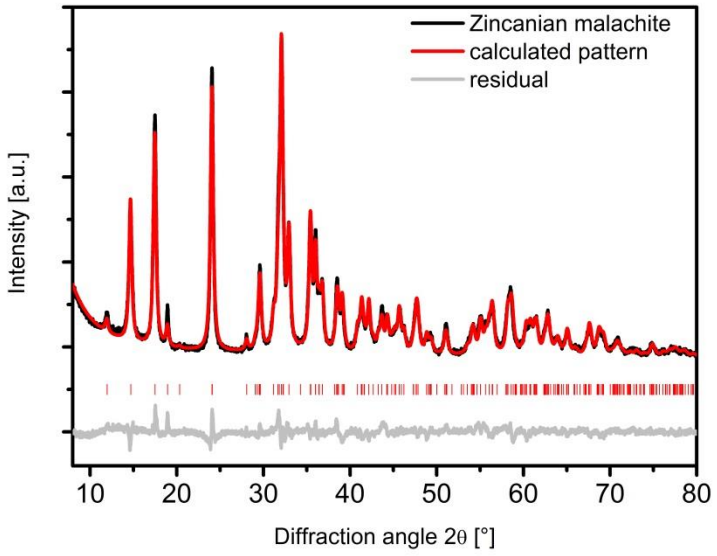

Fig. SI1 and SI2. Rietveld refinements for the XRD pattern of the Cu,Zn hydroxycarbonate precursor sample with Cu/Zn ratio of 40/60 (#12630) and 80/20 (#12716), experimental data (black), total calculated curve (red), background (light grey), difference curve (grey). The tick marks indicate the positions of the Bragg reflections.

Table SI1. Structural data and technical details of the Rietvield refinements

	Cu:Zn 40:60, (12630)	Cu:Zn 80:20, (12716)
formula	$(Cu_{0.4}Zn_{0.6})_5(CO_3)_2(OH)_6$	$(Cu_{0.8}Zn_{0.2})_2(CO_3)(OH)_2$
Phase	**Aurichalcite (100%)**	**Zincian Malachite (100%)**
Spacegroup	P121/m1	P121/a1
a (Å)	13.811	9.418
B (Å)	6.430	12.051
C (Å)	5.279	3.2018
β	101.10	96.9
Cryst size L (nm)	18.0	26.9
LVol-IB (nm)	11.5	17.1
Preferred orientation order	6	6
Background order	4	4
Correction (zero error)	-0.847	-0.022
Rwp	10.783	8.362